

CHARACTERISTICS OF ENERGY-OPTIMAL SPIRALING LOW-THRUST ESCAPE TRAJECTORIES

Nicholas Bradley*, Daniel Grebow†

We present and discuss trajectory characteristics of low-thrust spacecraft thrusting along the instantaneous velocity vector toward escape. The behavior of the osculating eccentricity is examined, in which eccentricity decreases to a minimum before quickly increasing toward escape ($e = 1$). We find that the argument of periapsis replaces true anomaly as the fast time variable, and the spacecraft escapes near an osculating true anomaly of 90 degrees. This behavior was observed by the authors while designing thrusting maneuvers for the Dawn spacecraft. In this paper the dynamical theory governing these observations is discussed and explored with numerical simulations.

INTRODUCTION

Spacecraft that utilize high efficiency low-thrust engines (which deliver a thrust magnitude on the order of tens to hundreds of milli-Newtons) are increasingly being utilized to accomplish a variety of mission objectives that may otherwise not be possible to achieve. As the technology develops, the algorithms used to design and execute low-thrust spacecraft trajectories are maturing as well. In this paper, we describe the characteristics of a certain type of low-thrust trajectory: the locally energy-optimal spiral.

Low-thrust escape is instantaneously energy-optimal when thrusting along the velocity vector. Many authors have investigated spiral-out escape for low-thrust spacecraft, ranging from introducing the concept at the beginning of the space age, to more recent efforts to introduce optimization strategies, targeting methods, and analytical approximations.¹⁻⁸

An energy-optimal control law was used to design the maneuver to transfer the Dawn spacecraft to a higher altitude orbit around the dwarf planet Ceres during extended mission operations in 2016-2017, and it was during this time that the authors observed the unique behaviors described in this paper. Driven by this operational experience, we explore here some of the idiosyncrasies of designing a trajectory to quickly spiral toward or away from a target body.

When designing the spiral-out transfer maneuver for Dawn, the Navigation team noticed that the osculating eccentricity would oscillate and decrease to a minimum value, and then increase to escape (if thrusting was allowed to continue through an escape condition). After some investigation,

*Outer Planet Navigation Group, Mission Design and Navigation Section, Jet Propulsion Laboratory, California Institute of Technology. 4800 Oak Grove Drive, Pasadena, California, 91109

†Outer Planet Mission Analysis Group, Mission Design and Navigation Section, Jet Propulsion Laboratory, California Institute of Technology. 4800 Oak Grove Drive, Pasadena, California, 91109

the team found that the exhibited characteristics are present in the dynamical theory that governs the motion of low-thrusting spacecraft around a single point-mass, and previous authors have noted similar effects (both analytic and numerical) to varying degrees.⁹⁻¹¹ Petropoulos investigated spiral-out behavior in-depth in a theoretical sense, and described the behavior of the eccentricity as a spacecraft approaches escape.¹² Petropoulos et al also described various control laws for low-thrust escape spirals, including the tangential thrust direction.¹³

With motivation from the actual as-flown Dawn trajectory, we describe the dynamical theory behind these observations and explore with numerical simulations the behavior of a low-thrust spacecraft thrusting toward escape with a locally energy-optimal control law. This paper builds on the rich history of investigation into the characteristics and behavior of low-thrust spirals.

MOTIVATION: DAWN TRANSFER TO XMO3 ORBIT

To satisfy the Dawn project's extended mission science requirements,¹⁴ the spacecraft transferred up to a high-altitude orbit, known as "XMO3" (eXtended Mission Orbit 3) in October-November 2016. In early October, the Dawn Navigation team designed the maneuver to raise the orbit radius from 2,000 km to an orbit with a periapsis altitude of at least 7,200 km, which was the only orbit requirement for XMO3 (this minimum altitude was required in order for the Gamma Ray and Neutron Detector instrument to gather background noise measurements intended to calibrate data collected during the prime mission). Because there were no requirements on the characteristics of the orbit other than the minimum altitude, the Navigation team utilized a locally energy-optimal steering law to design the transfer. The designed spiral-out is shown in Figure 1.

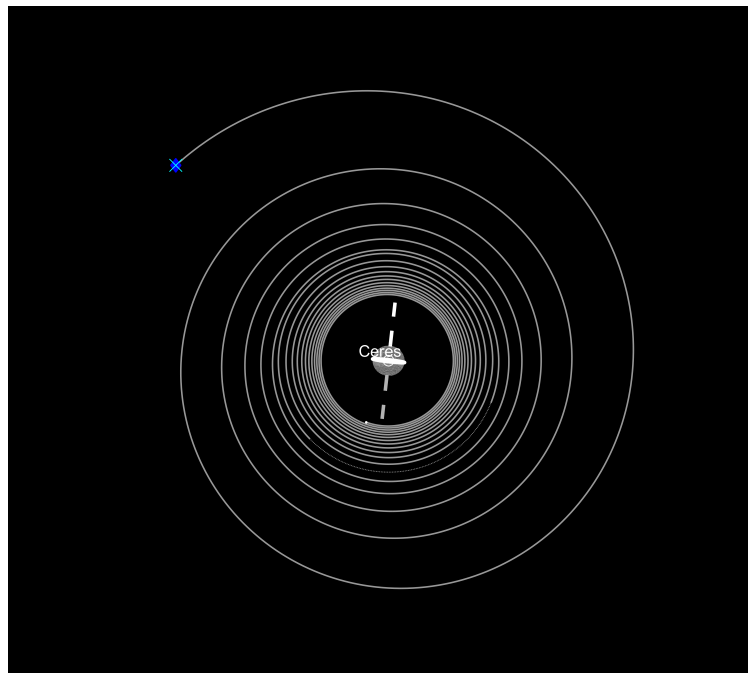


Figure 1. Dawn spacecraft spiraling transfer to the XMO3 orbit as part of the extended mission; the blue x is the location of the XMO3 orbit insertion. The gap in the spiral near the bottom center is a forced coast segment inserted for a required High Gain Antenna track, when the spacecraft was not allowed to thrust.

The orbit radius for the spiral-out transfer, along with osculating periapsis and apoapsis, is shown

in Figure 2 plotted as a function of transfer time. The plot indicates the typical Keplerian motion for the first 20 days of the transfer, where the orbit radius passes between periapsis and apoapsis as the spacecraft true anomaly rotates through a full 360 degrees (i.e., the green line oscillates between the blue and red lines, touching them when the spacecraft crosses an apse). However, after 20 days into the transfer, the orbit radius no longer touches the osculating ellipse apses. This interesting phenomenon is perhaps better visualized by inspecting true anomaly as a function of time.

In the top plot in Figure 3, the true anomaly ‘settles’ near 90 degrees roughly 20 days into the transfer. Concurrently, the argument of periapsis starts rotating about the unit circle, replacing the true anomaly as the fast time variable. At this time, the spacecraft ceases traversing the full extent of the osculating ellipse. Here it is sufficiently far away from Ceres that the thrust acceleration, compared to the central body gravity, is large enough to continuously turn the ellipse a full 360 degrees. Also during this time, the eccentricity reaches a minimum (see Figure 4) and increases toward escape ($e = 1$). In actual operations, thrusting to enter the high orbit ceased at around $e = 0.1$, well before the spacecraft could escape from Ceres.

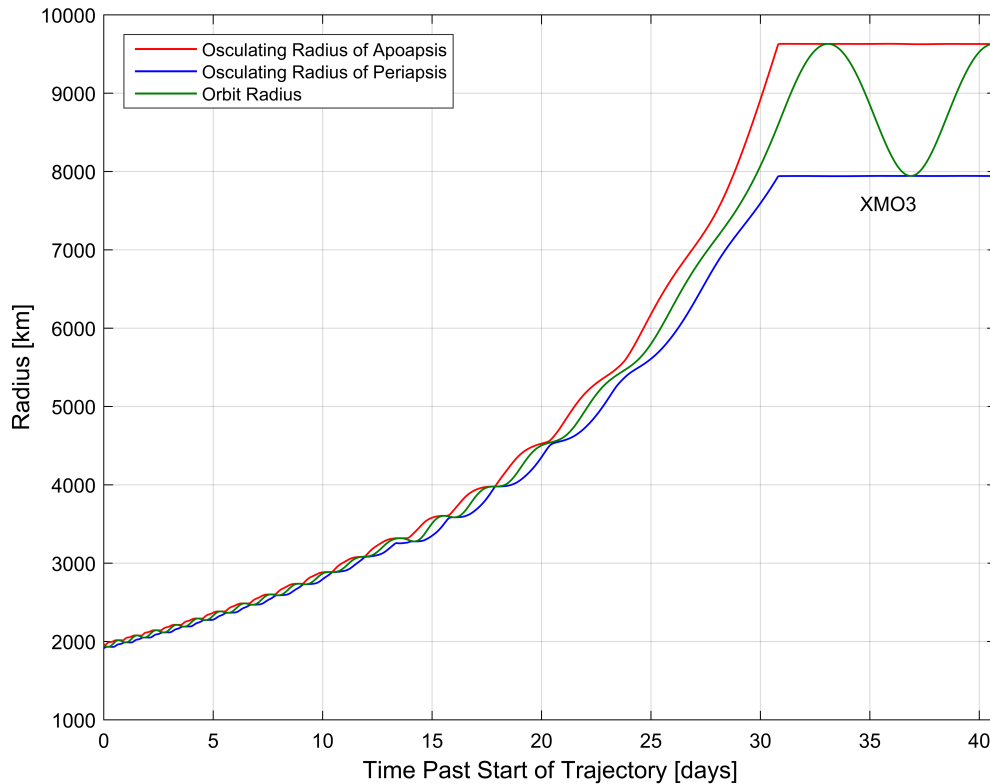


Figure 2. Dawn spacecraft spiral-out to the XMO3 orbit; radius (green), osculating periapsis (blue) and osculating apoapsis (red) are shown as a function of transfer time.

Also shown in Figure 4 is a High Gain Antenna (HGA) pass, when the spacecraft ceased thrusting in order to communicate with operators on the ground. The Navigation team initially thought that the behavior of the osculating eccentricity increasing as thrust progressed was due to the placement of this forced coast period. It was hypothesized that perhaps the coasting occurred at a location

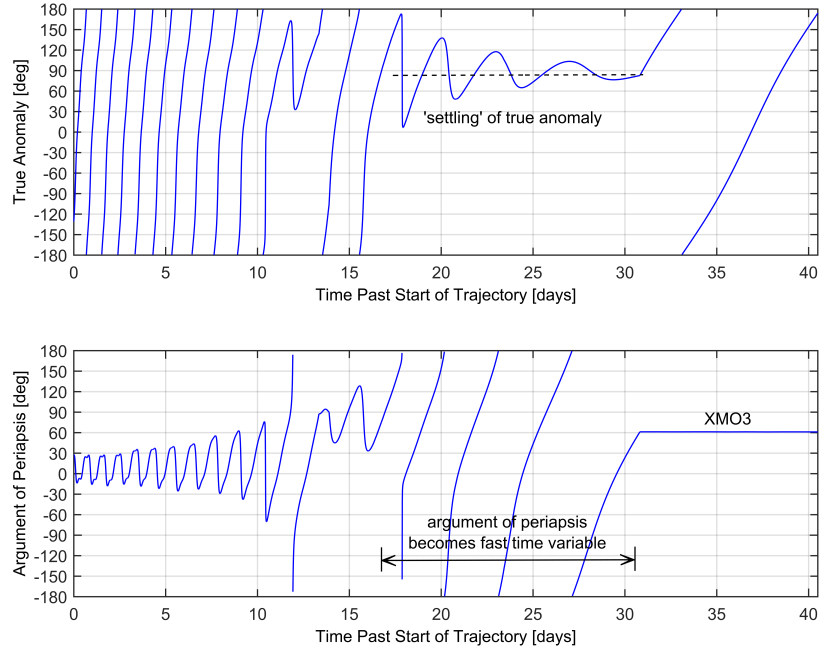


Figure 3. Dawn spacecraft spiral-out to the XMO3 orbit; true anomaly and argument of periapsis are shown as a function of transfer time.

in the orbit such that the subsequent thrust “reinforced” the increasing eccentricity, similar to how apoapsis may be raised (and eccentricity increased) by thrusting only through periapsis. However, after theoretical investigation (described in later sections of this paper), the team realized that such behavior is characteristic of locally energy-optimal spirals for low-thrust trajectories even when thrusting is continuous (i.e. no coasting). The presence of the HGA pass simply breaks the spiral into two parts. It is apparent that before the HGA pass, at about 10 days past the start of the trajectory, the osculating eccentricity reached a minimum near zero and subsequent local minima then began to increase. However, the HGA pass effectively re-started the spiral-out from a different true anomaly in the orbit, and the osculating eccentricity then decreased to a new minimum near zero (around 17 days) before proceeding toward escape.

THEORETICAL OBSERVATIONS OF LOW-THRUST SPIRALS

To better understand the interesting behavior observed during the Dawn spacecraft spiral-out to the XMO3 orbit, we investigated the orbital theory behind this phenomenon by studying well-known orbital mechanics equations and by performing numerical simulations.

In the following general analysis, it is assumed that a spacecraft is thrusting in the instantaneous velocity direction. Since thrusting is entirely in-plane, no out-of-plane component is considered in the analysis. The analysis also assumes that no external forces act in the out-of-plane direction; gravity is assumed to be from a central point-mass, and no other external influences (solar radiation pressure, third bodies, nonspherical gravity, etc.) are present. As indicated by the actual operational example of the Dawn spacecraft (where many perturbations are present), the behavior described in the following analysis does not significantly change in the presence of additional perturbations.

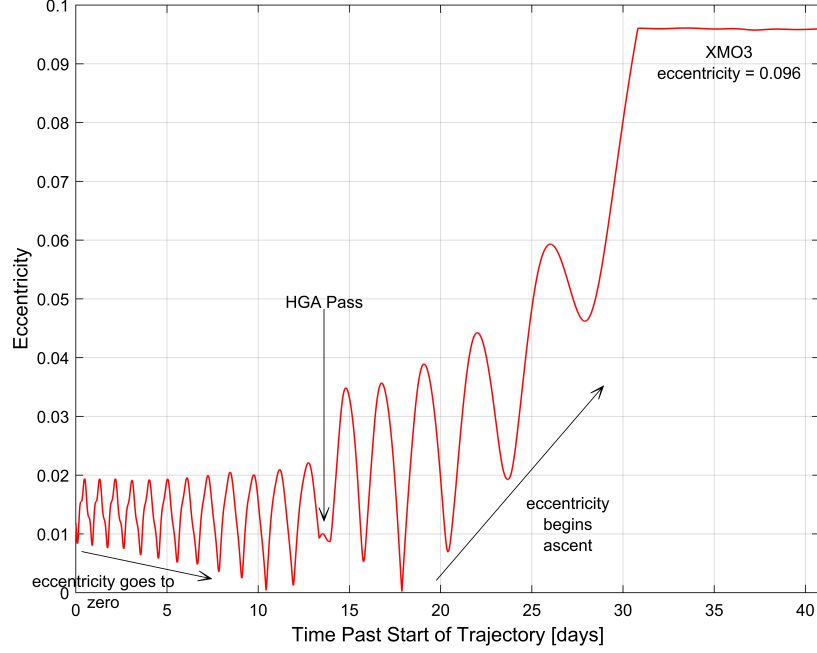


Figure 4. Dawn spacecraft spiral-out to the XMO3 orbit; eccentricity is shown as a function of transfer time.

Theoretical Analysis

Local Energy-Optimality. At any given time t , the most effective way to change a spacecraft's specific energy (that is, to either minimize or maximize \dot{E}) is to thrust either parallel or anti-parallel to the instantaneous velocity vector. This optimality is easily shown by examining the osculating specific energy equation (Equation 1).

$$E(t) = \frac{v^2}{2} - \frac{\mu}{r} \quad (1)$$

where v is the magnitude of the instantaneous velocity, μ is the gravitational parameter of the central body, and r is the magnitude of the instantaneous position vector with respect to the central body's center. Converting Equation 1 into a vector equation gives:

$$E = \frac{1}{2}(\mathbf{v} \cdot \mathbf{v}) - \mu(\mathbf{r} \cdot \mathbf{r})^{-\frac{1}{2}} \quad (2)$$

where \mathbf{v} is the instantaneous velocity vector, and \mathbf{r} is the instantaneous position vector. Differentiating this equation once with respect to time, and defining the instantaneous total acceleration vector as \mathbf{a} yields:

$$\dot{E} = (\mathbf{v} \cdot \mathbf{a}) + \mu(\mathbf{r} \cdot \mathbf{r})^{-\frac{3}{2}}(\mathbf{r} \cdot \mathbf{v}) \quad (3)$$

If the total acceleration is due only to the gravitating central body, the two terms in Equation 3 cancel, which results in $\dot{E} = 0$ (one of the ten constants of two-body spacecraft motion). For a spacecraft with a thruster, we may separate the total acceleration into its gravitational component

\mathbf{a}_g and thrust component \mathbf{a}_T so that $\mathbf{a} = \mathbf{a}_g + \mathbf{a}_T$. Performing this substitution and cancelling equivalent terms leaves us with:

$$\dot{E} = \mathbf{v} \cdot \mathbf{a}_T \quad (4)$$

To maximize \dot{E} , it is evident that the thrust acceleration and the velocity vector must be aligned. So, for \dot{E} -maximal escape, the thrust must be aligned with the instantaneous velocity vector. Likewise, for \dot{E} -minimal capture and spiral-down, the thrust vector must be exactly opposite the instantaneous velocity vector. (Another way to show that thrusting along or against the velocity vector is instantaneously energy-optimal is to consider when ΔE is an extremum for an instantaneous thrusting impulse $\Delta \mathbf{v}$ and take the limit as $\Delta t \rightarrow 0$.)

Reduced Gauss equations for along-velocity thrusting. Because the orbit is at all times contained within a single plane (see assumptions above), only four orbital elements are needed to describe the spacecraft's orbit: semimajor axis (a), eccentricity (e), argument of periapsis, which we use as the angular orientation of the orbit (ω), and true anomaly, which measures the spacecraft's angular location in its orbit relative to the osculating periapsis (f).

Gauss' variational equations provide an analytic representation of the first time derivatives of the orbit elements when a spacecraft is exposed to an external nonconservative perturbing acceleration. The perturbing acceleration may be expressed in terms of its radial component a_r and its component in the angular direction a_θ , which is perpendicular to the radial direction. Note also that in three-dimensional space, a component along the angular momentum direction a_h may be included, but is not considered here for the planar spiral.

With these considerations, Gauss' variational equations are written as below (adapted from Battin¹⁵). Here, $h = \sqrt{\mu p}$ is the scalar angular momentum of the orbit, and $p = a(1 - e^2)$ is the semiparameter, or semilatus rectum, of the orbit. Note also that the expression for \dot{f} has a secular variation expression as its first term, which accounts for the motion of the spacecraft about the osculating orbit.

$$\dot{a} = \frac{2a^2}{h} \left(e \sin(f) a_r + \frac{p}{r} a_\theta \right) \quad (5)$$

$$\dot{e} = \frac{1}{h} \left(p \sin(f) a_r + ((p + r) \cos(f) + r e) a_\theta \right) \quad (6)$$

$$\dot{\omega} = \frac{1}{h e} \left(-p \cos(f) a_r + (p + r) \sin(f) a_\theta \right) \quad (7)$$

$$\dot{f} = \frac{h}{r^2} + \frac{1}{h e} \left(p \cos(f) a_r - (p + r) \sin(f) a_\theta \right) \quad (8)$$

The following substitution permits a rotation of the basis frame from polar coordinates (r, θ) to the (n, v) direction, where the acceleration components are aligned with the velocity vector (a_v), and the in-plane vector orthogonal to both the velocity vector and the out-of-plane angular momentum vector (this orthogonal acceleration component is denoted as a_n).

$$\begin{pmatrix} a_r \\ a_\theta \end{pmatrix} = \frac{1}{\sqrt{1 + e^2 + 2e \cos(f)}} \begin{bmatrix} 1 + e \cos(f) & e \sin(f) \\ -e \sin(f) & 1 + e \cos(f) \end{bmatrix} \begin{pmatrix} a_n \\ a_v \end{pmatrix} \quad (9)$$

Using this transformation, and assuming that all of the disturbing acceleration is in the a_v direction (so that all coefficients of a_n are zero), and denoting as a_T the magnitude of the acceleration due to

the thrust on the spacecraft, we arrive at these reduced and modified versions of Gauss' equations:

$$\dot{a} = 2a^2 a_T \sqrt{\frac{2 + 2e \cos(f)}{\mu p} - \frac{1}{\mu a}} \quad (10)$$

$$\dot{e} = 2a_T (e + \cos(f)) \left[\frac{\mu(2 + 2e \cos(f))}{p} - \frac{\mu}{a} \right]^{-1/2} \quad (11)$$

$$\dot{\omega} = \frac{2a_T \sin(f)}{e} \left[\frac{\mu(2 + 2e \cos(f))}{p} - \frac{\mu}{a} \right]^{-1/2} \quad (12)$$

$$\dot{f} = \frac{h(1 + e \cos(f))^2}{p^2} - \frac{2pa_T \sin(f)}{he\sqrt{1 + e^2 + 2e \cos(f)}} \quad (13)$$

These four equations are a set of coupled differential equations, where only ω does not appear in the differential equations for the other three orbital elements. These equations assume that the thrust acceleration is a constant quantity. In reality, when a spacecraft is commanded at a certain thrust level, the force of the thrust is constant. Because the mass of the spacecraft drops as the thrust continues, the acceleration actually increases over time for a constant force.

To circumvent this assumption, a fifth differential equation may be included for the mass loss, where T is the constant force magnitude of the thruster and m is the mass of the spacecraft:

$$a_T = \frac{T}{m}, \quad \dot{m} = \text{negative constant} \quad (14)$$

Equation 14 is uncoupled from Equations 10-13 and can be analytically integrated. The resulting expression may then be substituted into Equations 10-13, and the coupled differential equations may be numerically integrated, much the same as a set of Cartesian states may be integrated according to the two-body equations of motion.

Analytical Observations. The eccentricity reaches a minimum or maximum when $\dot{e} = 0$ in Equation 11. There are only two ways that this can happen:

$$\dot{e} = 0 \text{ if } \begin{cases} e + \cos(f) = 0 \\ \text{or} \\ \frac{\mu(2+2e \cos(f))}{p} - \frac{\mu}{a} = 0 \end{cases} \quad (15)$$

The first condition is quite obviously a valid condition for a minimum or maximum; when $f = \cos^{-1}(-e)$, the eccentricity is at an extremum.

The second condition reduces nicely to the following quadratic:

$$1 + 2e \cos(f) + e^2 = 0 \quad (16)$$

This quadratic does not have any real roots for e , and therefore does not admit a real solution to the condition for $\dot{e} = 0$. So the first condition in Equation 15 is the only real solution for extrema in eccentricity.

In every spiral-out case, the eccentricity eventually reaches a final minimum, and then increases (though local minima may still occur) through $e = 1$ (see examples in later sections). This final minimum is the final true anomaly where $f = \cos^{-1}(-e)$ is satisfied. Thereafter, the true anomaly oscillates around an asymptotic value, rather than "wrapping around" the unit circle. Since the true anomaly can no longer reach this condition for eccentricity extremum, the eccentricity increases without bound.

Numerical Explorations

All of the following simulated trajectories are generated using the constant parameters listed in Table 1. The thrust direction is always parallel to the instantaneous velocity vector.

Table 1. Constant Parameters for All Spiral-Out Thrust Simulations

Parameter	Value
Gravitational parameter (μ)	62.63 km ³ /s ²
Initial spacecraft mass (m_0)	800 kg
Constant thrust force (F)	25 mN
Constant mass flow rate (\dot{m})	-5.0 g/hr

Single Spiral Example. A single spiral-out trajectory is generated with the initial conditions given in Table 2.

Table 2. Initial Conditions for Single Spiral Example

Parameter	Initial Value
Semimajor axis (a_0)	2000 km
Eccentricity (e_0)	0.2
Argument of Periapsis (ω_0)	90 deg
True anomaly (f_0)	0 deg

When these initial conditions and thrust parameters are integrated to escape (equivalently when the instantaneous specific orbit energy is zero, the semimajor axis goes to infinity, or the eccentricity reaches 1.0), the resulting spiral is shown in inertial space in Figure 5.

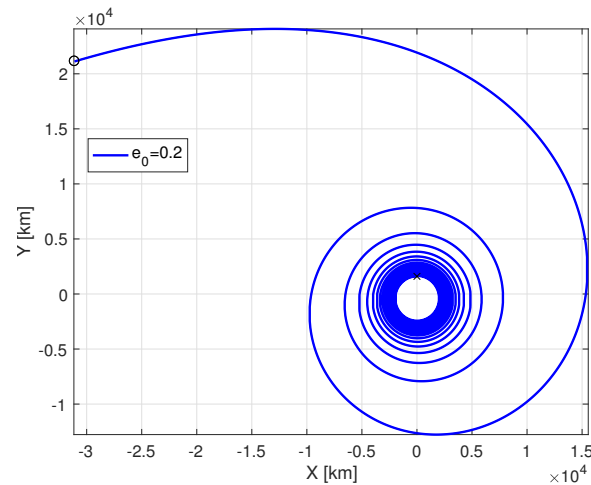


Figure 5. A single spiraling trajectory integrated to escape, inertial frame

An important and elucidating way to view the trajectory is to construct the spacecraft position in an *osculating perifocal* frame. A perifocal frame is a frame whose XY plane is coincident with the orbit plane, and the $+X$ axis points toward osculating periapsis. At any given instant in a

spiral-out trajectory, an osculating perifocal frame may be constructed by determining the osculating true anomaly of the spacecraft, which is its angular location relative to the osculating periapsis. The spacecraft's osculating perifocal coordinates may be found using Equation 17, where r is the osculating position magnitude and f is the osculating true anomaly.

$$\begin{bmatrix} x \\ y \end{bmatrix}_{peri} = r \begin{bmatrix} \cos(f) \\ \sin(f) \end{bmatrix} \quad (17)$$

After performing this coordinate transformation at each time step, the low-thrust spiraling example in Figure 5 is shown in the osculating perifocal frame in Figure 6.

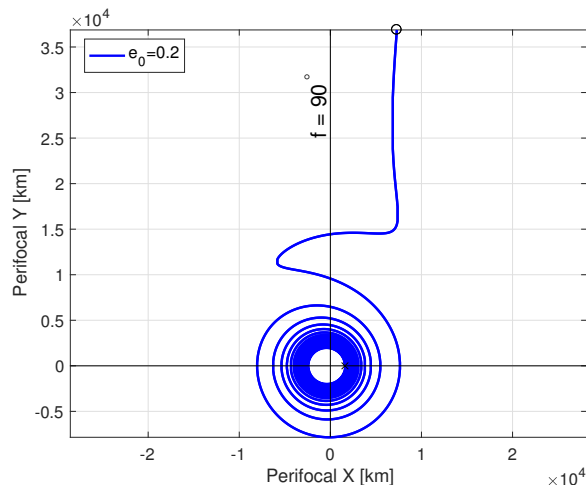


Figure 6. A single spiraling trajectory integrated to escape, osculating perifocal frame

It is apparent in Figure 6 that at some point, the spacecraft no longer reaches apoapsis (in the $-X$ direction). Escape occurs in a vertical direction, near a true anomaly of $f = 90^\circ$ (toward the $+Y$ axis). Because the spacecraft does not reach apoapsis, this means that the true anomaly ceases to traverse the unit circle, and is no longer the fast time variable. Because the true anomaly can no longer reach the condition specified by $f = \cos^{-1}(-e)$, the eccentricity increases without bound toward escape. Figure 7 shows the true anomaly, eccentricity, and argument of periapsis up to the time that the escape condition is met. The argument of periapsis begins nearly constant, but then begins to oscillate more with time. As soon as the true anomaly no longer reaches $f = 180^\circ$, the argument of periapsis becomes the fast time variable and starts wrapping around the unit circle. It appears that the time when this switching occurs also corresponds to the time when the osculating eccentricity reaches its global minimum before increasing to escape.

Varying Initial True Anomaly. We next investigate the behavior of the escape spiral when the initial true anomaly is varied around the unit circle and initial eccentricity is not varied. Table 3 gives the initial conditions for this example, where two initial eccentricities are examined.

Figures 8 and 9 show many escape spirals for two different initial eccentricities with initial true anomaly varying over the $[0, 360)$ deg range, all simultaneously plotted in an osculating perifocal frame. (The cyclical colormap in these figures is courtesy of Thyng et al¹⁶). All trajectories are numerically integrated to escape, where the integration is terminated.

Note here that the escape condition occurs near a true anomaly of $f = 90^\circ$ for both $e_0 = 0.2$ and $e_0 = 0.9$, regardless of the initial true anomaly in the eccentric orbit. Of course, the *inertial* escape

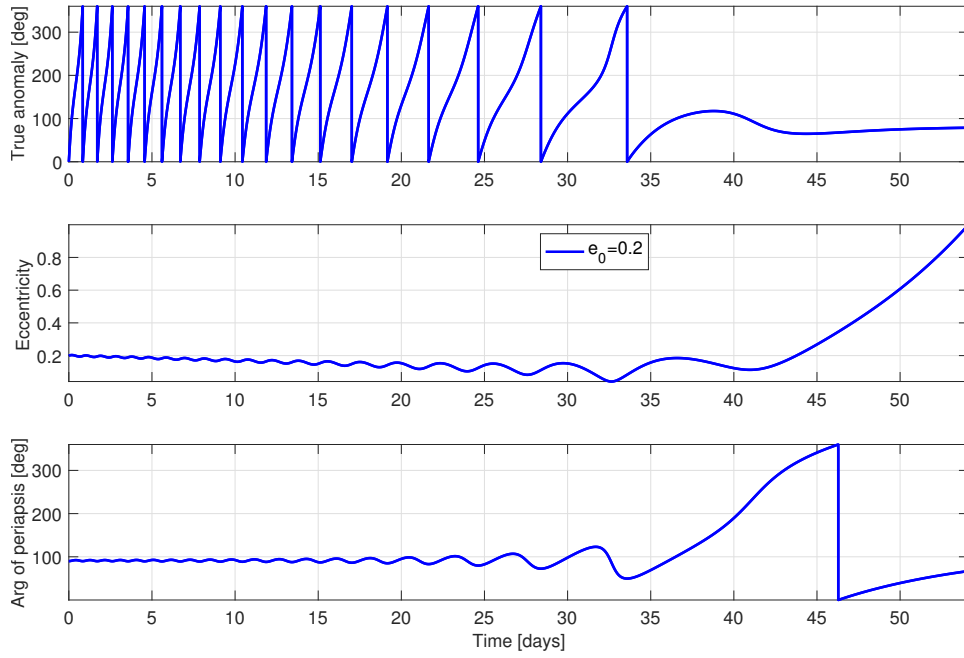


Figure 7. Orbital elements of a single spiraling trajectory integrated to escape

Table 3. Initial Conditions for Varying Initial True Anomaly Example

Parameter	Initial Value
Semimajor axis (a_0)	2000 km
Eccentricity (e_0)	0.2 or 0.9
Argument of Periapsis (ω_0)	90 deg
True anomaly (f_0)	varies over $[0, 360)$ deg

direction varies based on where the thrust begins in the initial orbit, but the osculating perifocal frame shows that the direction of escape relative to the osculating periapsis is nearly fixed. Figures 8 and 9 show that the behavior of escaping near $f = 90^\circ$ is independent of the starting true anomaly.

Varying Initial Eccentricity. Here, the behavior of the escape spiral is investigated when the spacecraft departs from periapsis, but the eccentricity of the initial orbit is allowed to vary. Table 4 gives the initial conditions for this example.

Table 4. Initial Conditions for Varying Initial Eccentricity Example

Parameter	Initial Value
Semimajor axis (a_0)	2000 km
Eccentricity (e_0)	varies over $[0, 0.9]$
Argument of Periapsis (ω_0)	90 deg
True anomaly (f_0)	0 deg

Figure 10 shows all escape spirals over the $[0, 0.9]$ range, all simultaneously plotted on an oscu-

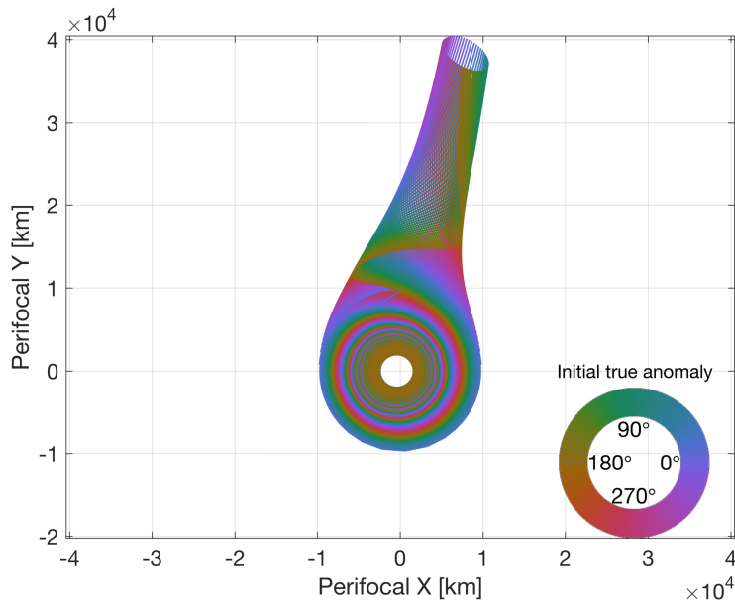


Figure 8. Spiral trajectories integrated to escape, varying initial true anomaly, $e_0 = 0.2$

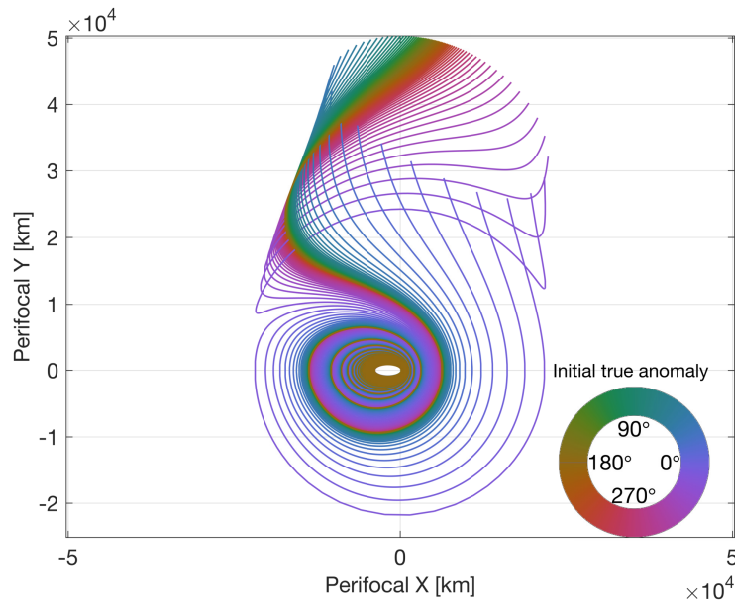


Figure 9. Spiral trajectories integrated to escape, varying initial true anomaly, $e_0 = 0.9$

lating perifocal plot. Again, the trajectories shown are numerically integrated until $e = 1$. Figure 11 shows the time history of the osculating eccentricity for various initial eccentricities. The simulations indicate that the spacecraft still escapes near $f = 90^\circ$ regardless of the initial eccentricity, although the size of the variation in final true anomaly depends on the initial eccentricity. Also,

from Figure 11 it is evident that no matter what the initial eccentricity is, even if it is initially quite large, the osculating eccentricity will still decrease to a global minimum at some time during the transfer. The time at which e is a minimum depends on the initial eccentricity of the orbit.

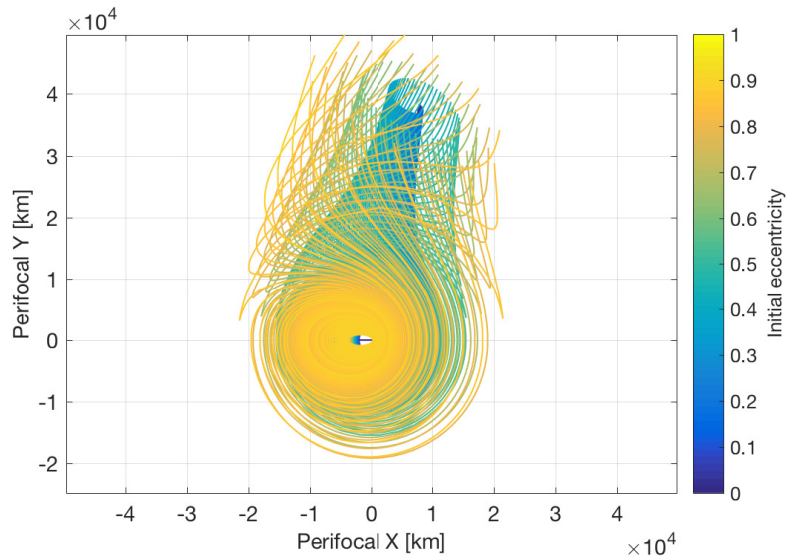


Figure 10. Spiral trajectories integrated to escape, varying initial eccentricity

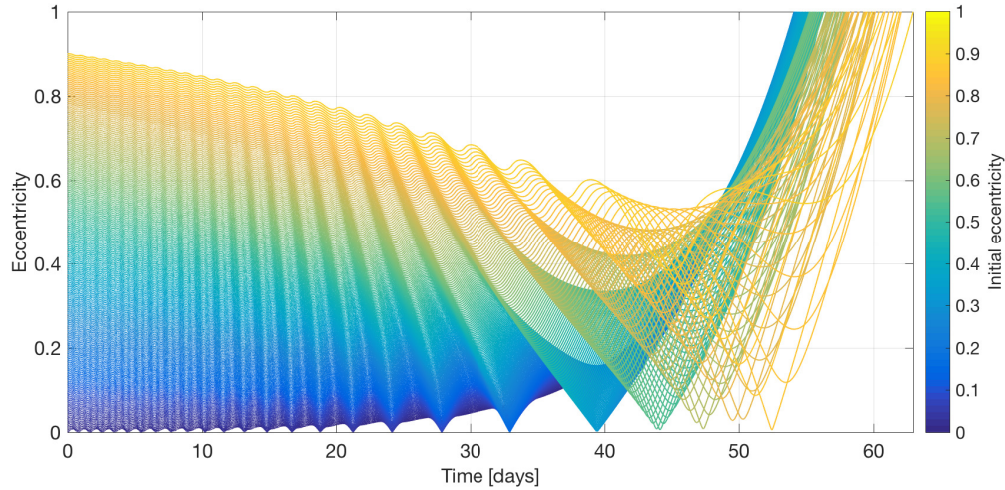


Figure 11. Eccentricity over time, varying initial eccentricity

Varying Initial Eccentricity and Initial True Anomaly. Finally, we present results when both initial eccentricity and initial true anomaly are allowed to vary. For a given initial orbital energy, the semimajor axis a_0 is fixed. We see from Gauss' variational equations (Equations 10-13) that the argument of periapsis ω does not appear in the expressions for the time rate of change of the other three elements (or, in other words, the initial orbit orientation has no effect on the evolution of the

other orbit elements). So, to explore spirals starting from orbits with a fixed initial energy, one needs only to vary the initial eccentricity e_0 and true anomaly f_0 . Here, an example spiral-out trajectory is integrated for each pair of values in a grid of e_0 and f_0 .

Instead of presenting all trajectories on an osculating perifocal plot, it is more insightful to examine the characteristics of the spirals via contour plots. Figure 12 shows the time needed to reach the escape condition with varying initial eccentricities and initial true anomalies. Figure 13 shows the overall minimum eccentricity reached on the way to escape for a given initial eccentricity and initial true anomaly.

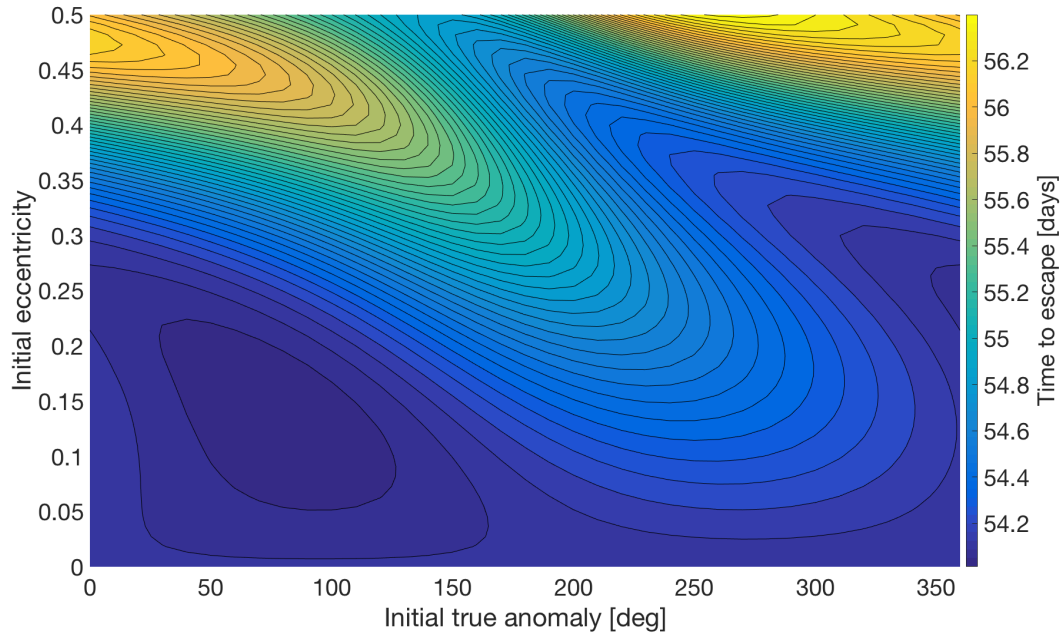


Figure 12. Time to reach escape condition, varying initial eccentricity and initial true anomaly

Characteristics and Observations

A very useful and insightful treatise on the analytically expected behavior of spiral-out trajectories is given by Petropoulos,¹² where the author performs a significant amount of averaging analysis to describe the behavior of the mean eccentricity and mean energy as the spacecraft proceeds toward escape. In the averaging analysis presented in that work, it is clearly shown that the mean eccentricity can be expected to decrease with an increase in orbital energy. It is also pointed out that the eccentricity must reach unity in a finite amount of time, corresponding to the time where $E = 0$, and so the mean eccentricity must therefore increase at some point. This line of reasoning shows that there must be a global minimum of the mean (and osculating) eccentricity of a spiraling trajectory as it proceeds toward escape.

The minimum eccentricity reached before increasing to escape varies depending on both the initial eccentricity and initial true anomaly (see Figure 13). The time at which this minimum occurs also varies. Figures 14 and 15 show the characteristics of the global minimum eccentricity where the initial true anomaly is zero (the spacecraft begins thrusting at periapsis) and the eccentricity of

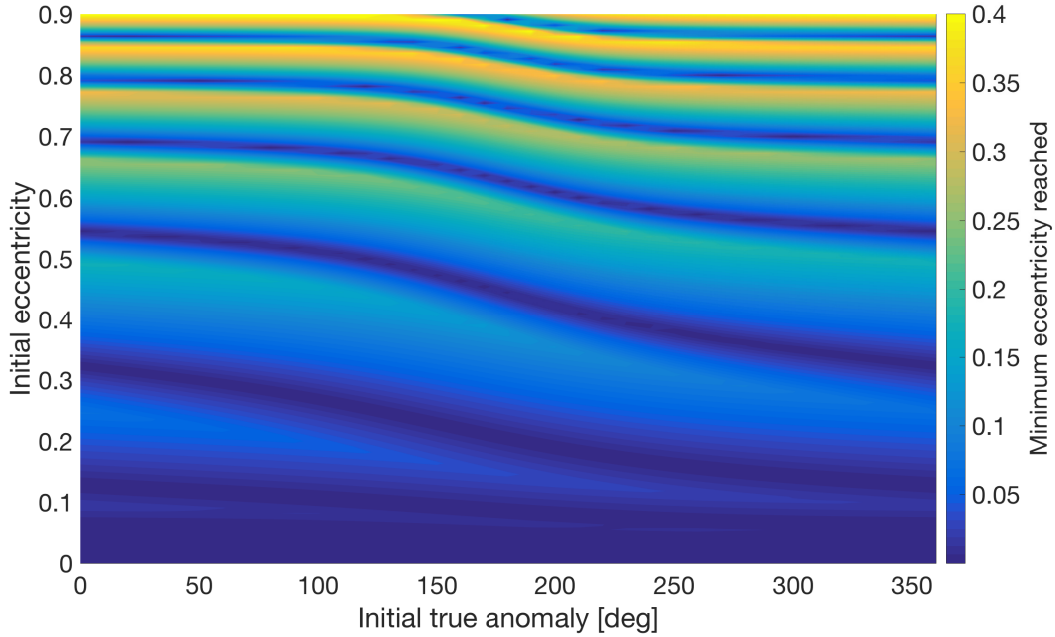


Figure 13. Minimum eccentricity reached during escape, varying initial eccentricity and initial true anomaly

the initial orbit is varied. It is clear that there are some initial eccentricities for which the global minimum eccentricity is very near zero, but other initial eccentricities produce a minimum eccentricity that can be quite large (yet still always smaller than the initial eccentricity for $e_0 > 0$). In general, the more circular an orbit is initially, the sooner the spacecraft will reach its global minimum eccentricity, but there are many local minima and maxima. Figure 13 shows the minimum eccentricity reached when the spacecraft is not constrained to begin at periapsis. There are multiple “bands” where the osculating eccentricity eventually reaches very near zero.

The time required to escape also varies significantly with initial condition. Figure 16 shows that when departing from periapsis, the time to escape varies by up to nine days (for this example problem) based on how eccentric the initial orbit is. Figure 12 shows this variation when considering different initial true anomalies. Interestingly, the global minimum escape time for these particular model parameters occurs at an initial eccentricity of $e_0 \approx 0.14$ and an initial true anomaly of $f_0 \approx 90^\circ$, not from an initially circular orbit and not from periapsis, as perhaps one might expect.

Another interesting observation comes by finding the initial true anomaly for a given initial eccentricity where escape is the fastest. That is, if optimally fast escape time is desired from a given orbit, where in the orbit should the spacecraft begin thrusting? Figure 17 shows the true anomaly at which thrust should begin if the fastest escape time is desired. (The time-optimal f_0 will be different for different constant parameters in Table 1.) As initial eccentricity increases, the time-optimal initial true anomaly wraps several times around the unit circle. Figure 12 shows that departing at the most sub-optimal initial true anomaly can cause a delay in the escape condition on the order of single days. Of course, the desired inertial direction of the escape asymptote is usually specified when a spacecraft escapes from a body, which dictates where in the initial orbit thrust should begin. Nevertheless, if all that is desired is fast spiral-up or spiral-down to a certain orbital energy, there

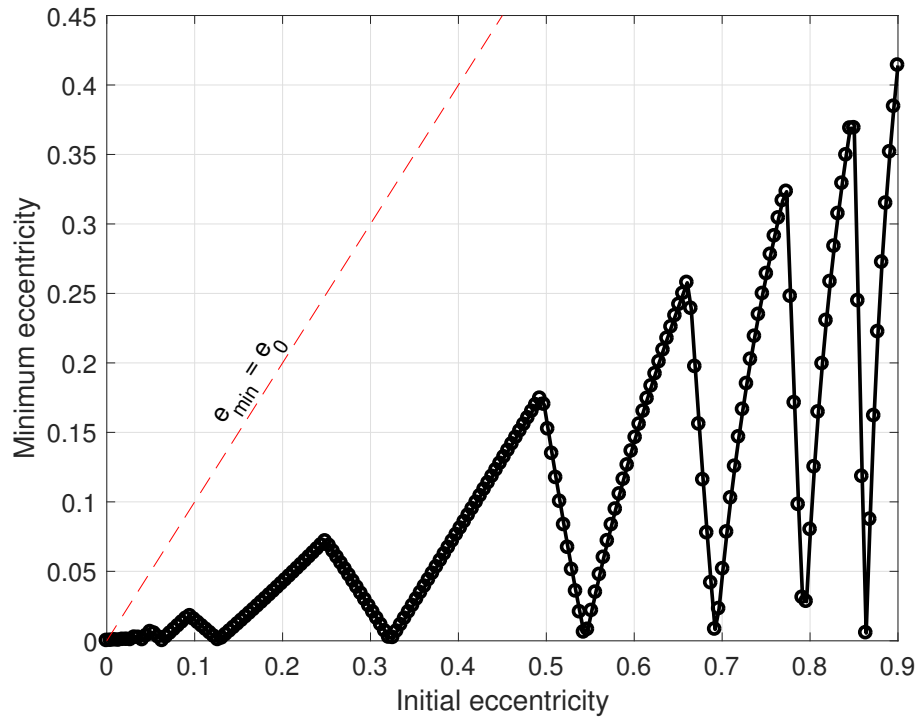


Figure 14. Global minimum eccentricity, varying initial eccentricity, $f_0 = 0^\circ$

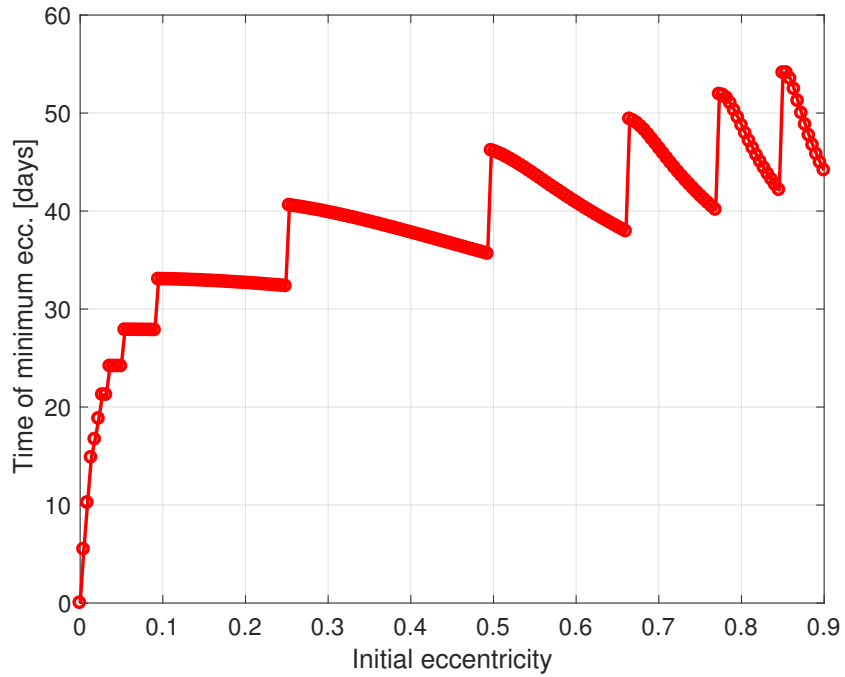


Figure 15. Time of global minimum eccentricity, varying initial eccentricity, $f_0 = 0^\circ$

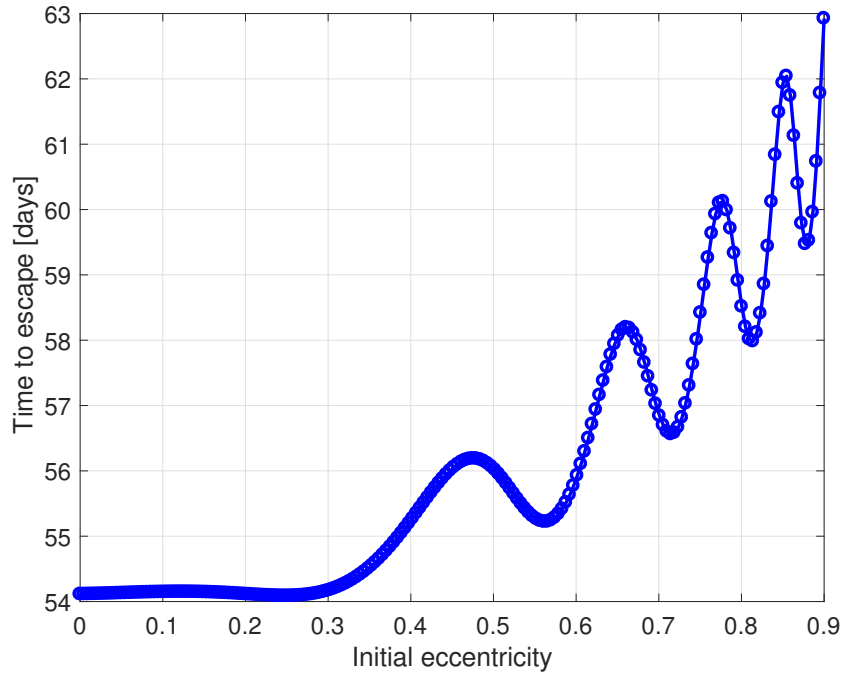


Figure 16. Time to escape, varying initial eccentricity, $f_0 = 0^\circ$

is a strong correlation of optimal completion time to initial true anomaly. This behavior was also described by Petropoulos.¹²

CONCLUSION

Low-thrust spiraling trajectories are instantaneously energy-optimal when the thrust is directed along the velocity vector. Assuming that no out-of-plane external forces act on the spacecraft, Gauss' variational equations reduce to four differential equations (five if including a non-constant spacecraft mass) that completely describe the motion of the spacecraft in classical orbit element space. As thrust proceeds toward escape, the osculating eccentricity decreases to a global minimum before quickly increasing to the escape condition. This minimum corresponds to the time when the spacecraft ceases to reach osculating apoapsis, and the fast time variable switches from true anomaly to argument of periapsis. Spiral-out trajectories always reach their escape condition near a true anomaly of $f \approx 90^\circ$, and the time needed to escape is highly correlated with the initial true anomaly for a given initial eccentricity.

The behavior described in this paper was seen in actual mission operations for the Dawn spacecraft. The designed and reconstructed Dawn trajectory, with full gravity and force models, show the expected characteristics described in this paper. While Dawn did not proceed all the way to escape on its spiral-out trajectory, the characteristics described by the variational equations are clearly present up to the time when thrust was stopped. To the authors' best knowledge, this is the first time that these theoretical and analytical observations of spiral-out trajectories, which have been studied for decades, have been observed on an actual operational deep-space mission.

While this behavior has been described theoretically, and now seen in actual operations, there

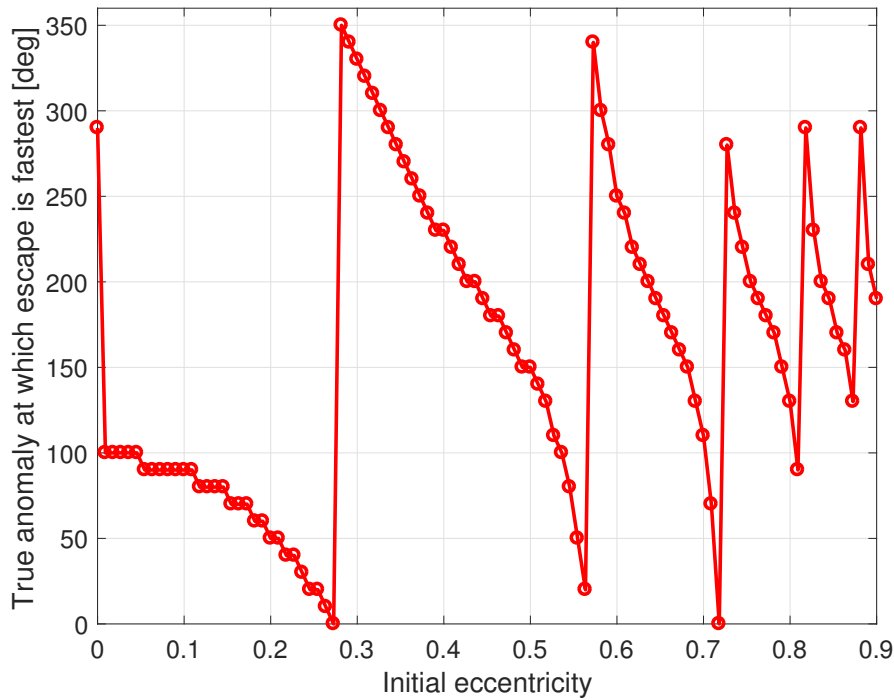


Figure 17. Initial true anomaly that produces the minimum escape time for a given initial eccentricity

are still unanswered questions regarding the nature of these spiral-out trajectories. Future areas of research could focus on what causes escape to always occur at a true anomaly near $f = 90^\circ$ (as opposed to some other value), what the connection is between the initial true anomaly and the time required to escape, and how to leverage these findings in future operational missions.

ACKNOWLEDGMENTS

The authors would like to thank Anastassios Petropoulos for his insight and encouragement in releasing these results, and for his very pertinent publication that preceded this paper. The authors also thank Gregory Whiffen for his review of the paper, and for his leadership on the Dawn maneuver design team.

This work was performed at the Jet Propulsion Laboratory, California Institute of Technology, under contract with the National Aeronautics and Space Administration. Government sponsorship acknowledged.

REFERENCES

- [1] H. Tsien, "Take-Off from Satellite Orbit," *Journal of the American Rocket Society*, Vol. 23, July-August 1953, pp. 233–236.
- [2] D. F. Lawden, "Optimal Programming of Rocket Thrust Direction," *Astronautica Acta*, Vol. 1, 1955, pp. 41–56.
- [3] D. F. Lawden, "Optimal Escape from a Circular Orbit," *Astronautica Acta*, Vol. 4, 1958, pp. 218–233.
- [4] D. Benney, "Escape From a Circular Orbit Using Tangential Thrust," *Journal of Jet Propulsion*, Vol. 28, March 1958, pp. 167–169.
- [5] F. M. Perkins, "Flight Mechanics of Low-Thrust Spacecraft," *Journal of the Aero/Space Sciences*, Vol. 26, No. 5, 1959, pp. 291–297.

- [6] H. M. Stark and P. D. Arthur, "Simple Approximate Solutions for Tangential, Low-Thrust Trajectories," *Journal of the Aerospace Sciences*, Vol. 28, November 1961, pp. 897–898.
- [7] Y.-Y. Shi and M. C. Eckstein, "Ascent or Descent from Satellite Orbit by Low Thrust," *AIAA Journal*, Vol. 4, December 1966, pp. 2203–2209.
- [8] Y.-Y. Shi and M. C. Eckstein, "An Approximate Solution for Ascending Low-Thrust Trajectories without Singularity," *AIAA Journal*, Vol. 5, January 1967, pp. 170–172.
- [9] C. Bombardelli, G. Baù, and J. Peláez, "Asymptotic solution for the two-body problem with constant tangential thrust acceleration," *Celestial Mechanics and Dynamical Astronomy*, Vol. 110, 2011, pp. 239–256.
- [10] J. A. Kechichian, "Low-Thrust Eccentricity-Constrained Orbit Raising," *Journal of Spacecraft and Rockets*, Vol. 35, No. 3, 1998, pp. 327–335.
- [11] J. A. Kechichian, "Orbit Raising with Low-Thrust Tangential Acceleration in Presence of Earth Shadow," *Journal of Spacecraft and Rockets*, Vol. 35, No. 4, 1998, pp. 516–525.
- [12] A. E. Petropoulos, "Some Analytic Integrals of the Averaged Variational Equations for a Thrusting Spacecraft," Tech. Rep. IPN Progress Report 42-150, California Institute of Technology - Jet Propulsion Laboratory, 2002.
- [13] A. E. Petropoulos, G. J. Whiffen, and J. A. Sims, "Simple Control Laws for Continuous-Thrust Escape or Capture and Their Use in Optimisation," *AIAA/AAS Astrodynamics Specialist Conference*, Monterey, California, August 5-8 2002.
- [14] M. D. Rayman, "Dawn at Ceres: The First Exploration of the First Dwarf Planet," *Proceedings of the 68th International Astronautical Congress*, In preparation. Adelaide, Australia, International Astronautical Congress, September 2017.
- [15] R. H. Battin, *An Introduction to the Mathematics and Methods of Astrodynamics*. American Institute of Aeronautics and Astronautics, Inc., revised ed., 1999.
- [16] K. Thyng, C. Greene, R. Hetland, H. Zimmerle, and S. DiMarco, "True colors of oceanography: Guidelines for effective and accurate colormap selection," *Oceanography*, Vol. 29, No. 3, 2016.